A Neutral Wave Observed in the Antarctic Polar Vortex

Yoshihiro TOMIKAWA

National Institute of Polar Research, Tokyo, Japan

Motoyoshi YOSHIKI

National Institute for Environmental Studies, Tsukuba, Japan

and

Kaoru SATO[1]

National Institute of Polar Research, Tokyo, Japan

(Manuscript received 21 July 2005, in final form 14 October 2005)

Abstract

An intensive radiosonde observation with time intervals of 3 h was performed in June 2002 at Syowa Station (39.6°E, 69°S) in the Antarctic. A wavelike disturbance with a wave period of 12–15 h, having a nearly barotropic structure was observed above a height of 22 km in the time period of 27–28 June 2002. A result of the hodograph analysis suggests that the short-period disturbance is not due to an inertia-gravity wave. A similar short-period disturbance is observed in the European Centre for Medium-Range Weather Forecasts (ECMWF) operational analysis data. Results of detailed analysis using the ECMWF data show that the short-period disturbance has a horizontal wavelength of about 2000 km, and propagates along a potential vorticity minimum region with a horizontal phase velocity of about 40 m s^{-1}. This phase velocity is equal to the background horizontal wind velocity at the potential vorticity minimum. A necessary condition for the barotropic instability is locally satisfied at the potential vorticity minimum. However, it is rather appropriate that the short-period disturbance is interpreted as a neutral wave than as an unstable wave in the barotropically unstable background flow. This result implies any unknown mechanism of the suppression of barotropic instability in the locally unstable background flow associated with a disturbed polar vortex.

1. Introduction

Charney and Drazin (1961) indicated that Rossby waves, with a zonal wavenumber larger than 3, are scarcely able to propagate into the middle and upper stratosphere [see also Scinocca and Haynes (1998)]. A winter polar vortex in the stratosphere is often accompanied by negative latitudinal gradients of zonal-mean potential vorticity (Leovy and Webster 1976; Manney et al. 1988), which satisfy a necessary condition for barotropic and baroclinic instabilities. Although these instabilities act as an in situ source of planetary-scale disturbances (Hartmann 1979, 1983), they are not an effective source of small-scale and short-period disturbances. Thus, waves with a small horizontal

Corresponding author: Yoshihiro Tomikawa, Polar Meteorology and Glaciology Group, National Institute of Polar Research, 1-9-10 Kaga, Itabashi-ku, Tokyo 173-8515, Japan.
E-mail: tomikawa@nipr.ac.jp

1 Present affiliation: Department of Earth and Planetary Science, The University of Tokyo, Tokyo, Japan.

scale (<3000 km), and a short wave period (<1 day), other than (inertia-) gravity waves, are not frequently observed in the middle and upper stratosphere.

There are few studies that examined disturbances with a small horizontal scale (<3000 km), and a short period (<1 day) in terms of waves other than (inertia-) gravity waves in the stratosphere. Tomikawa and Sato (2003) reported that the short-period disturbances with a period of 12–24 h are localized around the winter polar vortex edge in both hemispheres, and suggested that they are waves latitudinally trapped around the polar vortex edge, where the potential vorticity gradients are maximized. They have a zonal wavelength of about 2000 km, and a nearly barotropic structure.

In this paper, a short-period disturbance observed above a height of 22 km at Syowa Station (39.6°E, 69°S), in June 2002, is investigated in detail. The disturbance had a period of 12–15 h, a horizontal wavelength of about 2000 km, and a nearly barotropic structure, which are similar to those of the short-period disturbances analyzed in Tomikawa and Sato (2003). However, it is shown that this short-period disturbance observed at Syowa Station is interpreted as a neutral wave in the locally unstable background flow, while the short-period disturbances analyzed in Tomikawa and Sato (2003) owe their existence to large potential vorticity gradients around the polar vortex edge. Furthermore, dominance of the neutral wave over the unstable wave in the locally unstable background flow implies that the barotropic instability in the longitudinally limited unstable region associated with a disturbed polar vortex does not act as an effective in situ source of the short-period disturbances. Outlines of this paper are as follows: Details of the data and method of analysis used in this paper are described in section 2. The structure of short-period disturbance is analyzed using radiosonde data, and objective analysis data in section 3. Characteristics of the background flow are examined in terms of potential vorticity in section 4. A theoretical interpretation of the short-period disturbance is discussed using a quasigeostrophic potential vorticity equation in section 5. A summary and concluding remarks are given in section 6.

2. Data description and method of analysis

2.1 Radiosonde observation

An intensive observation with Vaisala RS80-15GH radiosondes was performed at Syowa Station (39.6°E, 69°S) in the time period from 20 through 30 June 2002 (Yoshiki et al. 2005). The Vaisala RS80-15GH radiosonde measures vertical profiles of atmospheric pressure, temperature, relative humidity, and zonal and meridional winds, using the Doppler shift of GPS radio wave. A total of 84 radiosondes was launched every 3 h during the observation period, and most of them reached an altitude higher than 28 km. In the extremely cold air, as in the polar stratosphere, the balloons burst earlier than in the normal condition, because the balloons deteriorate during the ascent. To prevent deterioration, the balloons were soaked in kerosene before the observation. The original data sampling time was ~2 s, and the ascent rate of the radiosondes was ~5 m s^{-1}. The data were interpolated at a constant vertical interval of 50 m to make analysis easier.

2.2 ECMWF operational analysis data

Detailed structure of the disturbance and its background field are analyzed, based on the European Centre for Medium-Range Weather Forecasts (ECMWF) operational analysis data, with a time interval of 6 h (0000, 0600, 1200, and 1800 UT). The data are distributed on a $2.5^\circ \times 2.5^\circ$ latitude and longitude mesh at 21 pressure levels (100, 70, 50, 30, 20, 10, 7, 5, 3, 2, and 1 hPa in the stratosphere). The analyzed time period is 21 days from 15 June to 5 July 2002. It should be noted that the radiosonde data analyzed here are not assimilated to the operational analysis.

2.3 Time filter

In order to extract the short-period disturbance, a high-pass filter with a cutoff period of 48 h is applied to the time series data following Tomikawa and Sato (2003). High-pass-filtered data can be contaminated by thermal tides, because the thermal tides have wave periods of 24 h and 12 h. Thus prior to extracting the short-period (<48 h) disturbance, the tidal components whose phases are fixed to local time are removed by subtracting the average of time series at each local time (0000, 0600, 1200,

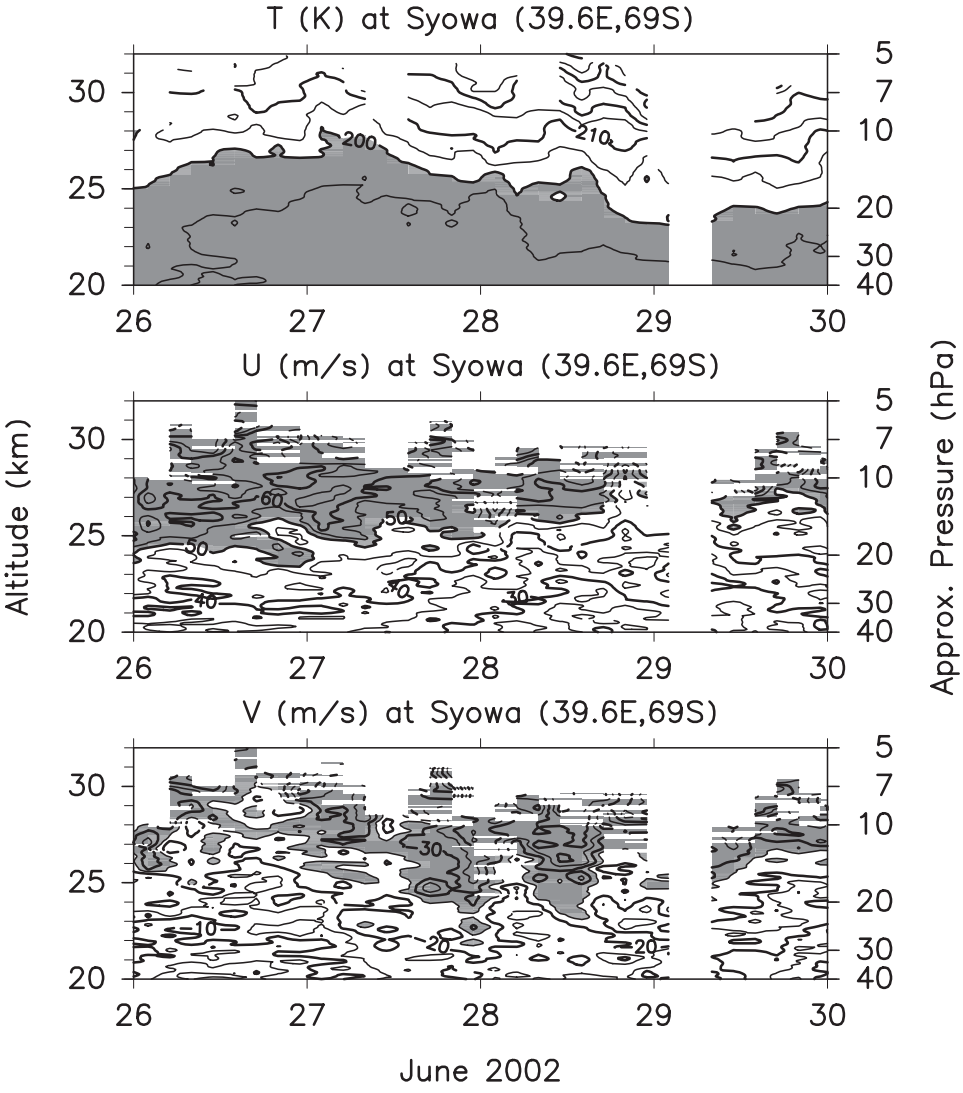

Fig. 1. Time-height sections of (top) temperature, and (center) zonal and (bottom) meridional winds measured by the radiosondes at Syowa Station in June 2002. Contour intervals are (top) 5 K and (center and bottom) 5 m s^{-1}. Regions with values (top) smaller than 200 K, (center) larger than 50 m s^{-1}, and (bottom) smaller than −25 m s^{-1} are shaded.

and 1800 UT) over the data period (i.e., 11 days for radiosonde data, and 21 days for ECMWF data) from each time series separately. Additionally, the data obtained by applying a low-pass filter with a cutoff period of 48 h to the ECMWF data are referred to as "background" data in this paper.

3. Structure of short-period disturbance

3.1 Results of radiosonde observations

Figure 1 shows time-height sections of temperature, and zonal and meridional winds obtained by the radiosonde observations at Syowa Station in June 2002. The lapse-rate tropopause and the temperature minimum are located around heights of 10 (not shown) and 20 km, respectively, and the temperature increases with height above a height of 20 km. The zonal wind velocity gets faster with height, in association with the polar-night jet. The meridional wind is southward above a height of 20 km during the observation period. A wave-like structure is seen in the meridional wind on 27 and 28 June 2002 (see the contour of

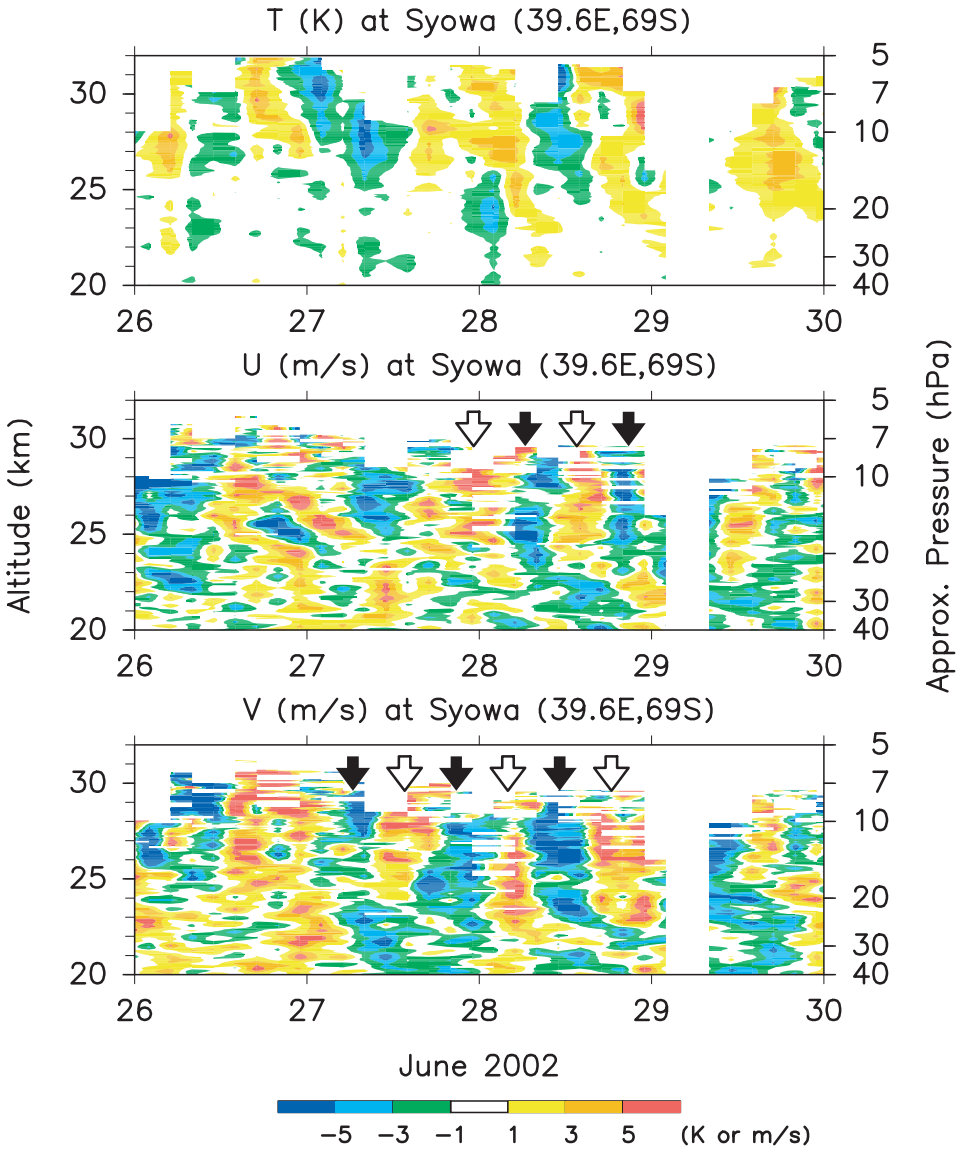

Fig. 2. The same as Fig. 1 except for the high-pass-filtered (<48 h) radiosonde data. Open and closed arrows represent positive and negative peaks, respectively, of zonal and meridional winds.

−25 m s^{-1}). The stratosphere before 26 June 2002 at Syowa Station, is characterized by vigorous gravity wave activity (not shown), which is described in detail by Yoshiki et al. (2005).

Figure 2 shows time-height sections of high-pass-filtered temperature, and zonal and meridional winds in the radiosonde data at Syowa Station. A wavelike structure, which has little phase tilt with height and a wave period of about 12 h, is seen above a height of 22 km in the zonal and meridional winds in the time period of 27–28 June 2002, though it is not seen in the temperature. Open and closed arrows in Fig. 2 represent positive and negative peaks, respectively, of zonal and meridional winds.

A downward propagating wavelike structure, with a wave period of about 1 day, is seen above a height of 24 km in the temperature from 26 through 29 June 2002. This temperature disturbance is not due to the short-period distur-

bance, observed in the zonal and meridional winds, and not discussed anymore in this paper.

3.1.a Possibility of inertia-gravity wave

An (inertia-) gravity wave is a possible candidate for the short-period (~12 h) disturbance in the stratosphere. However, the observed short-period disturbance is unlikely due to the (inertia-) gravity wave, from a hodograph analysis as shown in the following. The hodograph is defined as temporal and vertical variations of the horizontal wind vector. Parameters of the inertia-gravity wave can be estimated from the hodograph (Sato et al. 1997; Yoshiki and Sato 2000), using dispersion, polarization, and Doppler relations:

$$\frac{k^2}{m^2} = \frac{\hat{\omega}^2 - f^2}{N^2 - \hat{\omega}^2}, \quad \frac{a}{b} = \left|\frac{\hat{\omega}}{f}\right|, \quad \hat{\omega} = \omega - Uk, \quad (1)$$

respectively, where k and m are horizontal and vertical wavenumbers, respectively, a and b half lengths of the long and short axes of the ellipse fitted to the hodograph, respectively, f an inertial frequency, N a buoyancy frequency, ω and $\hat{\omega}$ ground-based and intrinsic frequencies of the wave, respectively, and U a background horizontal wind parallel to the long axis of the ellipse. Since, as shown in Fig. 2, the phase variation of the short-period disturbance with height is small, the hodograph in the temporal direction is used to estimate the parameters (e.g., Tomikawa et al. 2002). Figure 3 shows the hodograph of horizontal wind vectors, averaged over the height region of 24–28 km on 28 June 2002. The dotted line represents an ellipse fitted to the hodograph. The long axis of the ellipse points to the north-south direction. The ratio of long to short axis (a/b) is 1.4, and the ground-based wave period ($|2\pi/\omega|$) is 52200 s (= 14.5 h). The other parameters are estimated from the radiosonde data such as $N^2 \approx 5 \times 10^{-4}$ s^{-2}, $f = -1.36 \times 10^{-4}$ s^{-1}, and $U \approx -20$ m s^{-1}. The vertical wavelength ($= 2\pi/m$) estimated using (1) is smaller than 1 km. This value is much different from the observation seen in Fig. 2, indicating that the short-period disturbance is not due to the inertia-gravity wave.

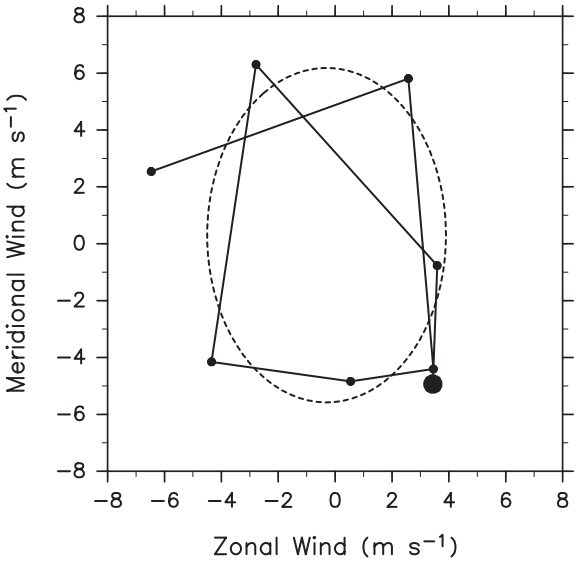

Fig. 3. Hodograph of the short-period disturbance observed at Syowa Station on 28 June 2002. Zonal and meridional wind components are averaged over the height region of 24–28 km. Large and small closed circles represent the horizontal wind vectors at the first time (0100 UT on 28 June 2002) and the other times, respectively. The dotted line shows an ellipse fitted to the hodograph.

3.2 Comparison with ECMWF data

Figure 4 shows time-height sections of temperature, zonal and meridional winds of the ECMWF data at the grid point (40°E, 70°S) closest to Syowa Station. The height region drawn in Fig. 4 is almost the same as that in Fig. 1, although the vertical coordinate in Fig. 4 is not the altitude but the log-pressure. The overall features of the ECMWF data are similar to those of the radiosonde data, both qualitatively and quantitatively. For example, the boundaries of shaded regions in Fig. 4 are located almost at the same altitude as those in Fig. 1 at any time (i.e., 200 K of temperature, 50 m s^{-1} of zonal wind, and −25 m s^{-1} of meridional wind). It is clear that a wavelike structure similar to the short-period disturbance in Fig. 1 is seen in the meridional wind of Fig. 4 in the time period of 27–28 June 2002.

The time-height sections made using the high-pass-filtered ECMWF data at the grid point (40°E, 70°S) closest to Syowa Station are shown in Fig. 5. A wavelike structure similar to that in Fig. 2 is seen in the meridional wind of

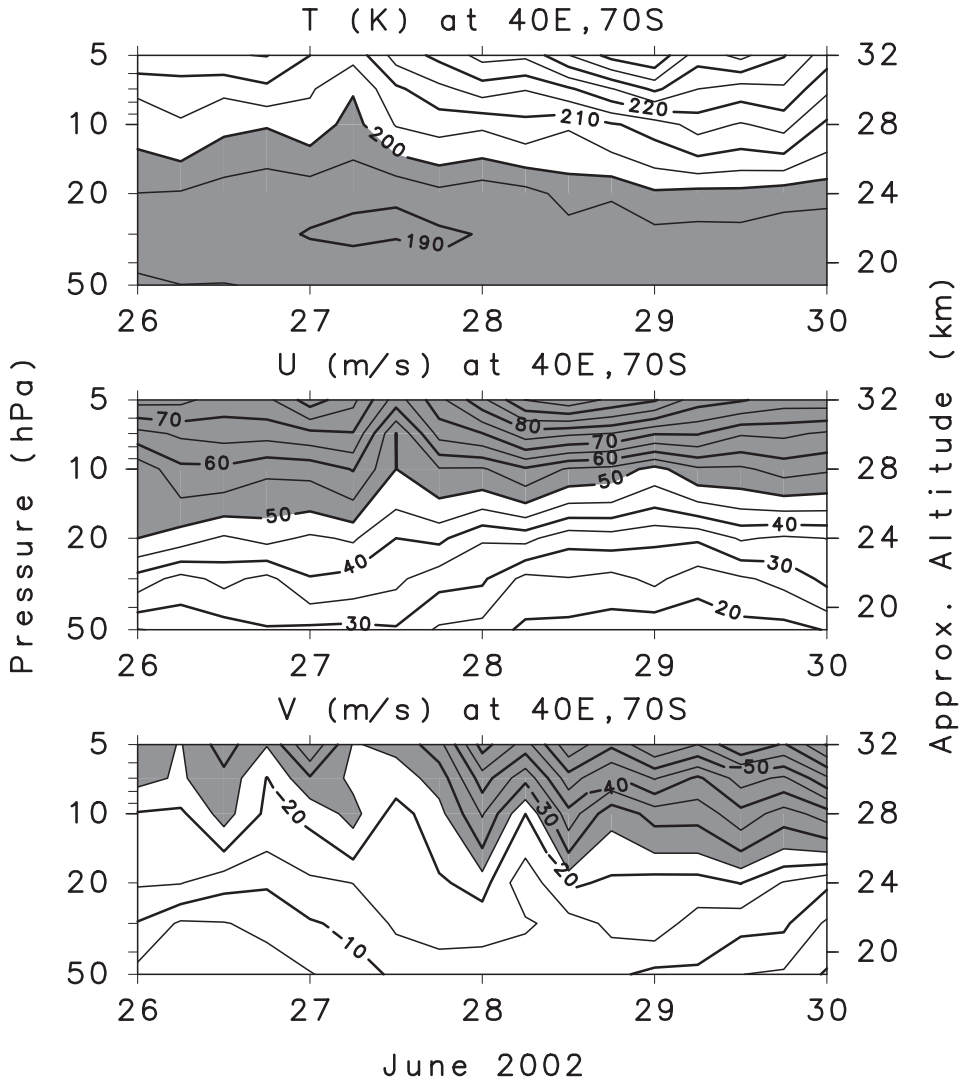

Fig. 4. The same as Fig. 1 except for the ECMWF data.

Fig. 5, though the wavelike structure of the zonal wind is not so clear as that of the meridional wind. The ECMWF data at the other three grid points surrounding Syowa Station have the same features (not shown). It is worth noting that a similar wavelike structure is also seen in the high-pass-filtered NCEP/NCAR Reanalysis data (not shown). See Kalnay et al. (1996) for details of NCEP/NCAR Reanalysis.

In order to examine the consistency between radiosonde and ECMWF data, and the phase relation between zonal and meridional wind disturbances, time variations of high-pass-filtered zonal and meridional winds of radiosonde data averaged over the height region of 24–28 km and those of ECMWF data averaged at the corresponding pressure levels of 20 and 10 hPa are shown in Fig. 6. Fluctuations seen in the radiosonde data accord well with those in the ECMWF data, both in amplitude and phase in the meridional wind from 1200 UT 27 to 0000 UT 29 June 2002, and in the zonal wind from 0000 UT 27 to 0000 UT 28 June 2002. The wave period is roughly 12–15 h. The phase of the zonal wind disturbance is about a quarter wave period ahead of that of the meridional wind disturbance. Note that zonal wind components are different between

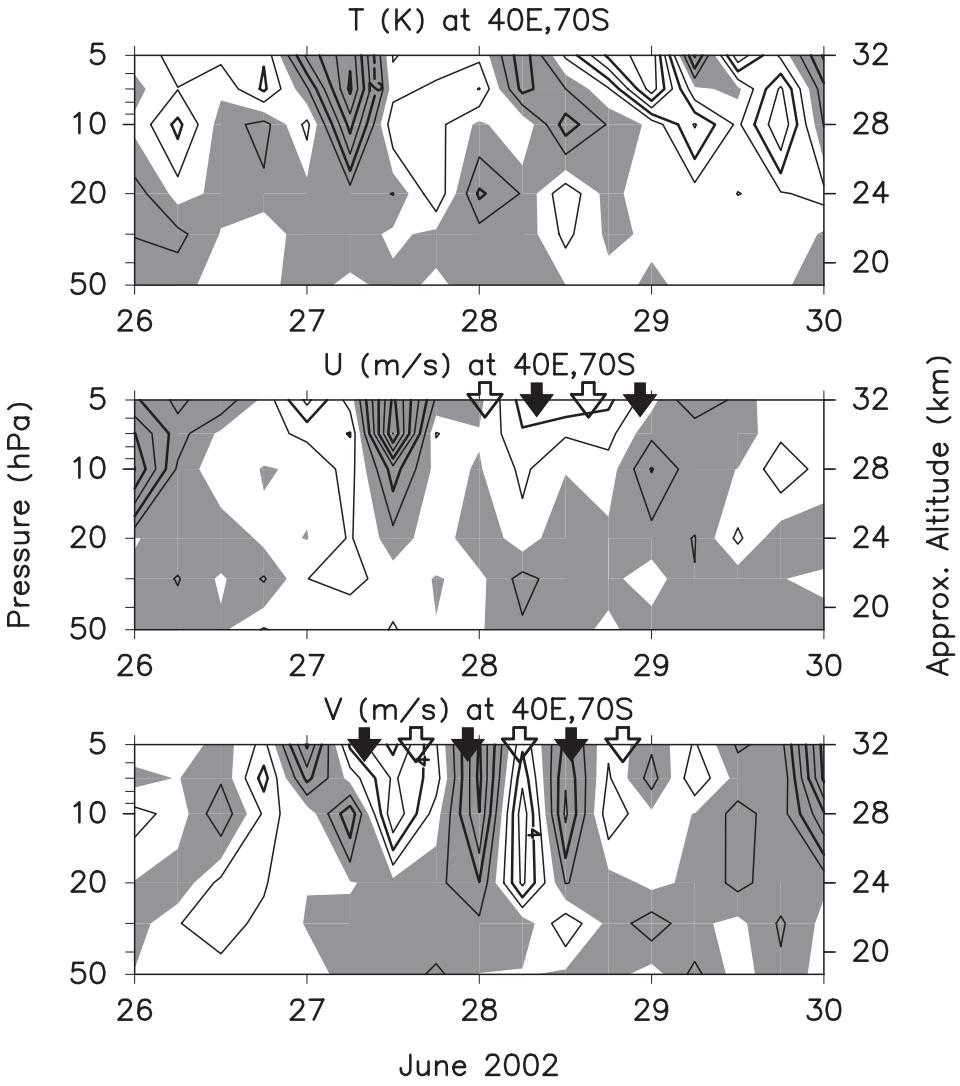

Fig. 5. The same as Fig. 2 except for the high-pass-filtered ECMWF data. Contour intervals are (top) 1 K and (center and bottom) 2 m s^{-1}. Contours of (top) 0 K and (center and bottom) 0 m s^{-1} are omitted. Negative values are shaded.

the radiosonde and ECMWF data from 0000 UT 28 to 0000 UT 29 June 2002. This discrepancy might be because a high-pass filter extracts not only the short-period disturbance, but also the product of the vertical shear of zonal wind and the altitude change with time on the pressure level.

3.3 Vertical structure

Figure 7 shows longitude-height sections of the high-pass-filtered meridional wind at 70°S, from 1200 UT 27 to 1200 UT 28 June 2002. A wavelike structure with a zonal wavelength of about 2000 km propagates eastward with a zonal phase velocity of about 40 m s^{-1}. This disturbance is seen above the pressure level of 20 hPa, and has a vertical scale greater than 10 km (i.e., 5–20 hPa). The disturbance basically has little phase tilt with height throughout the observed period, although the disturbance sometimes seems to tilt westward with height. A similar wavelike structure is seen also in the high-pass-filtered geopotential and relative vorticity data.

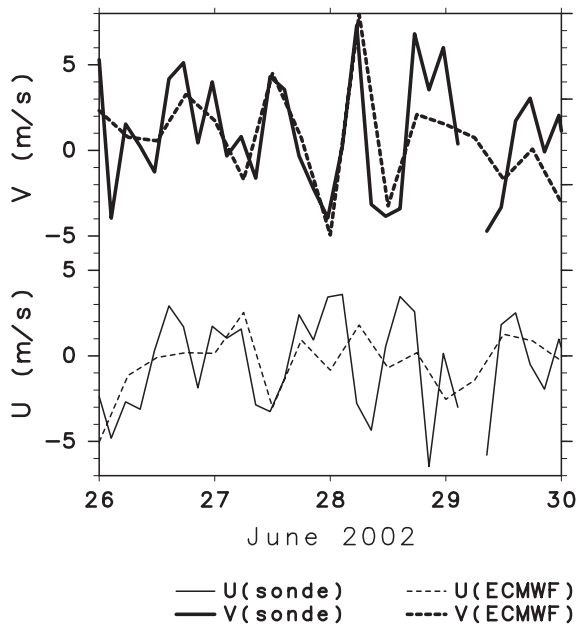

Fig. 6. Time variations of the high-pass-filtered (thin) zonal and (thick) meridional winds in the radiosonde data averaged over the height region of 24–28 km (solid) and in the ECMWF data averaged at pressure levels of 10 and 20 hPa (dashed).

3.4 Horizontal structure and propagation characteristics

In order to examine a horizontal structure of the short-period disturbance, polar stereographic projection maps of the high-pass-filtered meridional wind, and background potential vorticity on the 800-K isentropic surface from 0000 UT 27 to 0600 UT 28 June 2002 are made in Fig. 8. The 800-K isentropic surface was located around a height of 28 km and a pressure level of 10 hPa throughout the observation period. A potential vorticity in the hydrostatic approximation is given by (Hoskins et al. 1985)

$$P = -g(f\mathbf{e}_z + \nabla_p \times \mathbf{v}) \cdot \nabla_p \theta, \tag{2}$$

where P is the potential vorticity, g the gravity acceleration, $\mathbf{e}_z$ a unit vertical vector, ∇_p a three-dimensional gradient operator in xyp space, p a pressure, $\mathbf{v}$ a horizontal wind vector, and θ a potential temperature. The meridional wind disturbance, having a horizontal wavelength of about 2000 km, propagates eastward along the potential vorticity minimum region, surrounded by the thick solid lines in Fig. 8. The magnitude of meridional wind component of the disturbance is always maximized slightly poleward of the potential vorticity minimum. A phase tilt of the disturbance with latitude is small.

In order to examine a relationship between the horizontal phase velocity of the disturbance and the background horizontal wind, the air parcels are put along positive (65°W) and negative (40°W) peaks of the high-pass-filtered meridional wind every 1° latitude from 60°S to 75°S at 0000 UT on 27 June 2002, and adiabatically advected on the 800-K isentropic surface by the background horizontal winds, using the NIPR isentropic trajectory model (Tomikawa and Sato 2005) in Fig. 8. The air parcels put on the potential vorticity minimum propagate eastward together with the disturbance, indicating that the horizontal phase velocity of the disturbance is equal to the background horizontal wind velocity at the potential vorticity minimum. This feature is common to other isentropic surfaces between 600 K and 1000 K (not shown). On the other hand, the air parcels located equatorward and poleward of the potential vorticity minimum are advected faster and slower than the disturbance, respectively. This feature suggests that the short-period disturbance is not simply advected by the background horizontal wind, but has its own phase velocity as a wave.

4. Background potential vorticity field

Figure 9 shows a latitude-height section of the magnitude of background horizontal wind velocity at the longitude, where the positive peak of high-pass-filtered meridional wind is observed at each time from 0000 UT 27 to 0600 UT 28 June 2002. The equatorward edge of negative potential vorticity gradient region, which corresponds to the potential vorticity minimum, accords well with the 40 m s^{-1} contour of background horizontal wind velocity above the potential temperature of about 600 K in each panel of Fig. 9. The background horizontal wind velocity of 40 m s^{-1} is almost the same as the horizontal phase velocity of the disturbance estimated in section 3.3.

Figure 10a shows latitudinal distributions of potential vorticity on the 800-K isentropic sur-

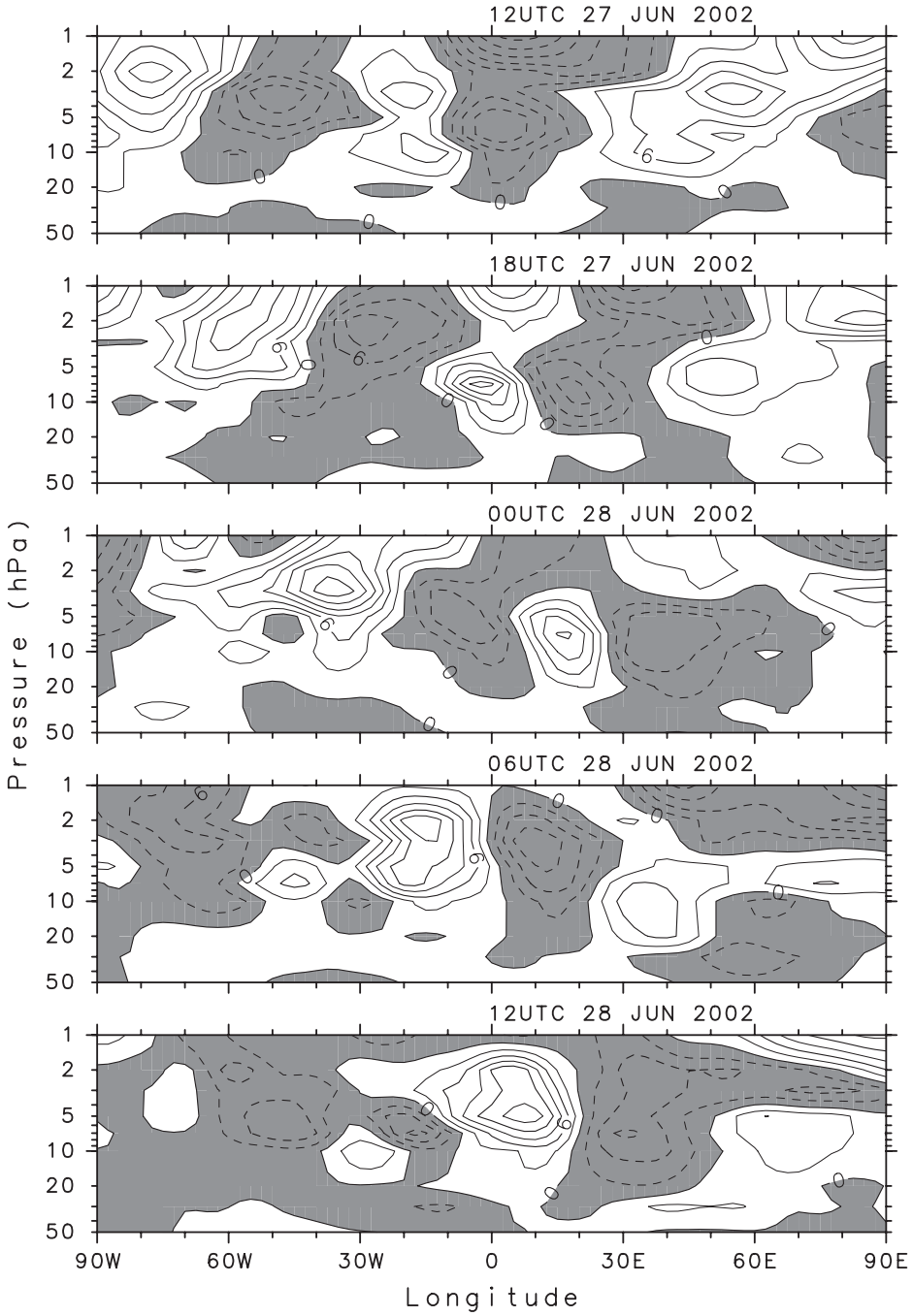

Fig. 7. Longitude-height sections of the high-pass-filtered meridional wind at 70°S from 1200 UT 27 to 1200 UT 28 June 2002. Contour intervals are 3 m s^{-1}. Negative values are shaded.

face at 1200 UT on 27 June 2002. Dotted and solid lines represent the potential vorticity averaged over the latitude belt (i.e., zonal-mean), and the longitude region of 90°W–30°E, where the short-period disturbance was clear and its phases were zonally aligned (Fig. 8), respectively. Although both of them have minima of potential vorticity at 65°S–70°S, the minimum

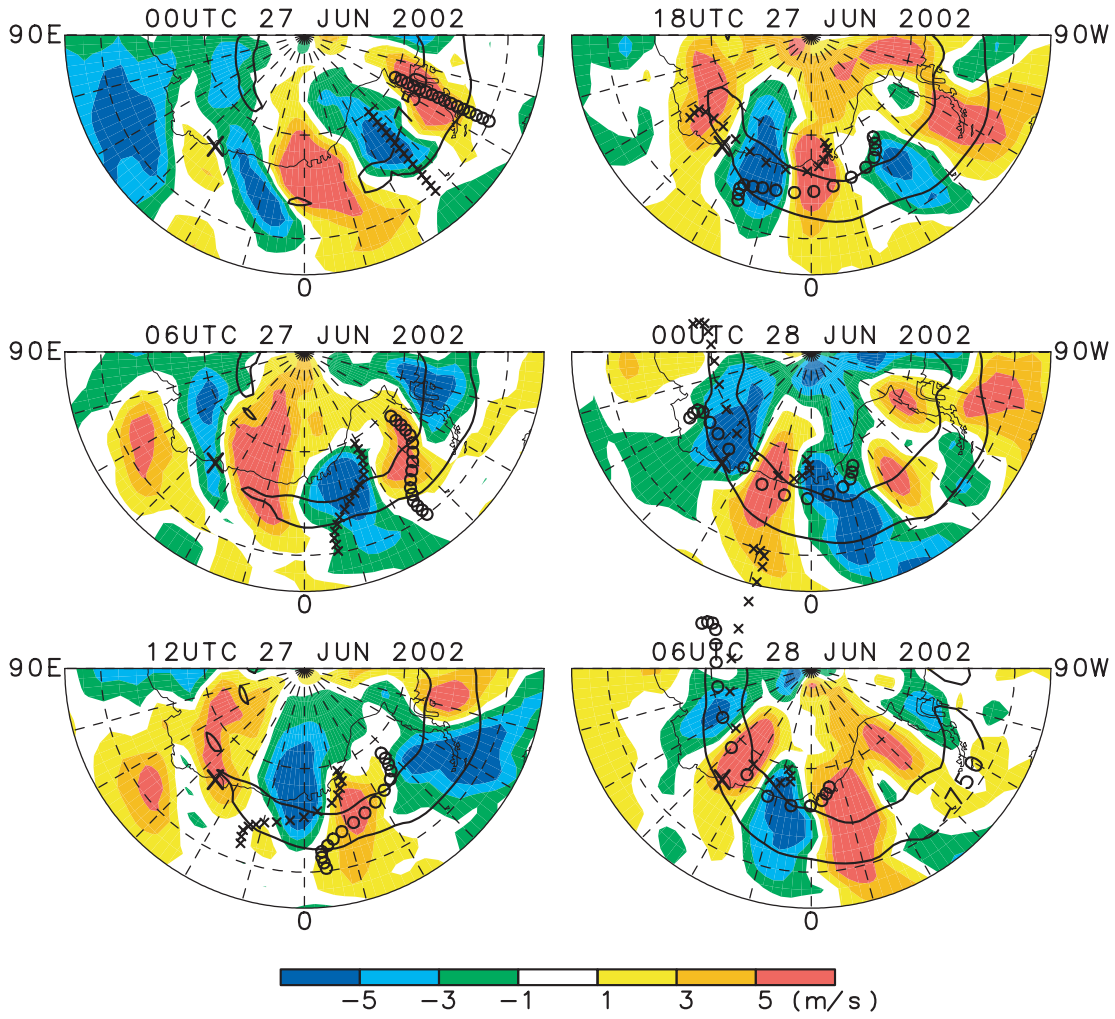

Fig. 8. Polar stereographic projection maps of (colors) the high-pass-filtered meridional wind on the 800-K isentropic surface from 0000 UT 27 to 0600 UT 28 June 2002. Large crosses represent the location of Syowa Station. Thick solid lines show the contours of −750 PVU (1 PVU = 10^{-6} K kg^{-1} m^2 s^{-1}) background potential vorticity. Small circles and crosses represent the locations of air parcels at each time, which were put along positive (65°W) and negative (40°W) peaks of the high-pass-filtered meridional wind, respectively, every 1° latitude from 60°S to 75°S at 0000 UT on 27 June 2002.

of potential vorticity averaged over 90°W–30°E is more intensified than that of zonal-mean potential vorticity. Then the magnitude of negative potential vorticity gradient at 70°S, shown in Fig. 10b, averaged over 90°W–30°E is much larger than that of negative zonal-mean potential vorticity gradient at 70°S. It is considered that such a difference results from zonal asymmetry of the potential vorticity distribution, associated with a planetary wave activity. The longitude region of 90°W–30°E at 1200 UT on 27 June 2002 is hereafter referred to as a reference longitude region.

5. Theoretical interpretation of the short-period disturbance

The reference longitude region discussed in the previous section satisfies a necessary condition for the barotropic instability, where the positive and negative potential vorticity gradi-

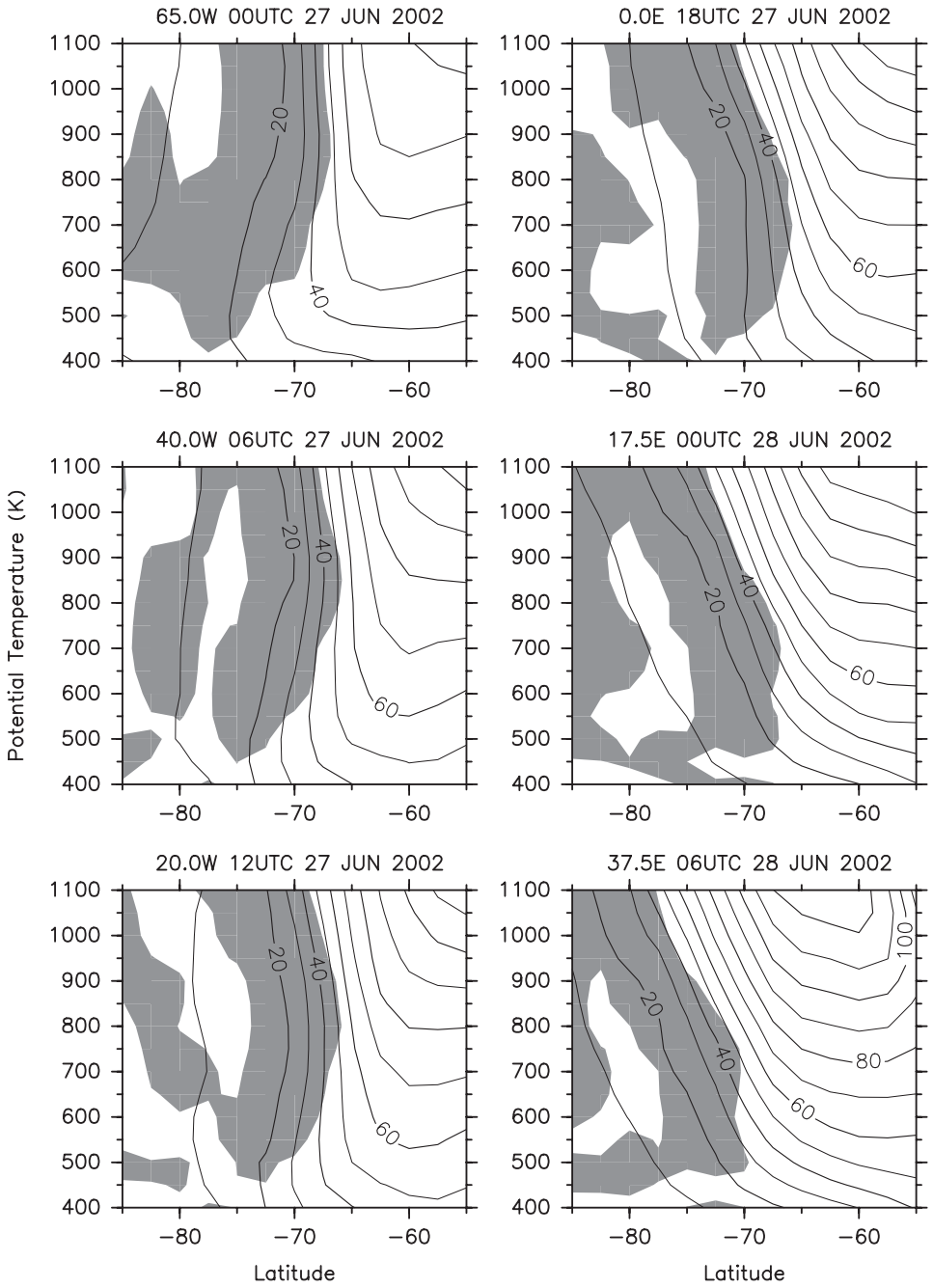

Fig. 9. Latitude-height sections of background horizontal wind along the positive peaks of the high-pass-filtered meridional wind at each time from 0000 UT 27 to 0600 UT 28 June 2002. Contour intervals are 10 m s^{-1}. Regions with negative potential vorticity gradients are shaded. A longitude at each time is given at top left of each panel.

ent regions are lying side-by-side (Kuo 1949, 1973). However, little phase tilt of the short-period disturbance in the latitudinal direction is inconsistent with a well-known phase structure of the barotropically unstable wave, whose phase tilts with latitude against the background wind shear. Instead, such a latitudinal structure with little phase tilt reminds us of a

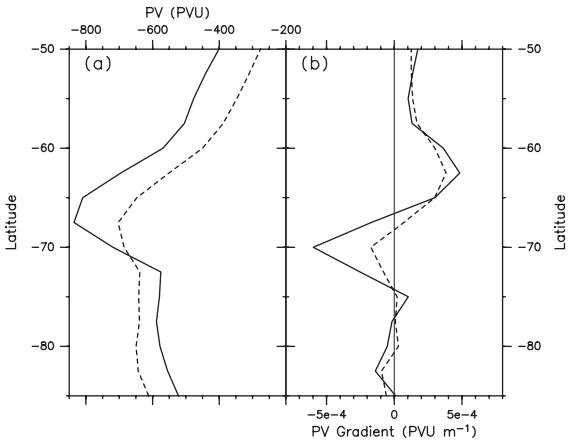

Fig. 10. Latitudinal distributions of (a) zonal-mean potential vorticity (dotted) and potential vorticity averaged over the longitude region of 90°W–30°E (solid) where the short-period disturbance was observed, and (b) zonal-mean potential vorticity gradient (dotted) and potential vorticity gradient averaged over 90°W–30°E (solid) on the 800-K isentropic surface at 1200 UT on 27 June 2002.

neutral wave having no phase tilt with latitude in the barotropically unstable flow (Dickinson 1973). In this section, it is shown that the short-period disturbance observed at Syowa Station can be interpreted as a neutral mode in a barotropically unstable shear flow.

Neutral and unstable mode solutions are analytically and numerically obtained, respectively, in the background zonal flow similar to the observation. For theoretical convenience, a quasigeostrophic potential vorticity (QGPV) equation in a background zonal flow ($\bar{u}$) is considered:

$$\left(\frac{\partial}{\partial t}+\bar{u}\frac{\partial}{\partial x}\right)(\psi_{xx}+\psi_{yy}+\rho_0^{-1}(\rho_0\varepsilon\psi_z)_z) + \psi_x(\beta-\bar{u}_{yy}-\rho_0^{-1}(\rho_0\varepsilon\bar{u}_z)_z)=0, \quad (3)$$

where ψ is a stream function of the disturbance, ρ_0 a density of the reference state, $\varepsilon \equiv f_0^2/N^2$, and $f_0+\beta y$ the Coriolis parameter. The term of $\beta-\bar{u}_{yy}-\rho_0^{-1}(\rho_0\varepsilon\bar{u}_z)_z$ represents a latitudinal gradient of QGPV. Since the observed disturbance has little phase tilt with height and a large vertical scale (>10 km), it is safely assumed that the disturbance is barotropic ($\partial\psi/\partial z=0$). Suppose a disturbance with a form of $\psi \equiv \mathrm{Re}[\Psi(y)\exp(ik(x-ct))]$, where c is a ground-based phase velocity, and k is a zonal wavenumber. Then (3) is written as (Rayleigh-Kuo equation, Rayleigh 1880; Kuo 1949)

$$\frac{d^2\Psi}{dy^2}+\left(\frac{\beta-\bar{u}_{yy}-\rho_0^{-1}(\rho_0\varepsilon\bar{u}_z)_z}{\bar{u}-c}-k^2\right)\Psi=0. \quad (4)$$

The boundary condition for Ψ is $\Psi=0$ as $y\to\pm\infty$.

5.1 *Quasigeostrophic and normalized potential vorticity distributions*

In order to compare the observed short-period disturbance with the neutral and unstable modes obtained from (4), realistic latitudinal distributions of background zonal wind and QGPV gradient in (4) need to be chosen. QGPV (q) is computed by (Andrews et al. 1987)

$$q=f+\mathbf{e}_z\cdot\nabla_p\times\mathbf{v}+\frac{f}{p}\frac{R}{H_0}\left(\frac{p}{N_0^2}(T-T_0)\right), \quad (5)$$

where $H_0=7$ km is a scale height, $z\equiv H_0\ln(p_s/p)$ (where $p_s=1000$ hPa) the log-pressure height, R the gas constant, and N_0 the buoyancy frequency of the reference state computed from T_0, which is defined as the zonal-mean temperature at 60°S averaged over the data period. Latitudinal distributions of zonal wind, QGPV, and QGPV gradient, averaged over the reference longitude region at 10 hPa at 1200 UT on 27 June 2002, are shown by dotted lines in Figs. 11a, 11b, and 11c, respectively. The zonal wind distribution is approximated by a hyperbolic tangent profile given by

$$\bar{u}(y)=\frac{U_{max}-U_0}{2}\left(1+\tanh\left(\frac{y-y_0}{L_y}\right)\right)+U_0, \quad (6)$$

where $U_{max}=70$ m s^{-1}, $U_0=10$ m s^{-1}, $y_0=67$°S (i.e., the midpoint of hyperbolic tangent profile), and $L_y=4.5$° latitude (= 500 km). The hyperbolic tangent zonal wind profile is shown by a dashed line in Fig. 11a.

A dashed-dotted line in Fig. 11c represents negative zonal wind curvature ($\equiv -\bar{u}_{yy}$), averaged over the reference longitude region at 10 hPa. It is found that the latitudinal variation of QGPV gradient at 10 hPa is mostly caused by that of the negative zonal wind cur-

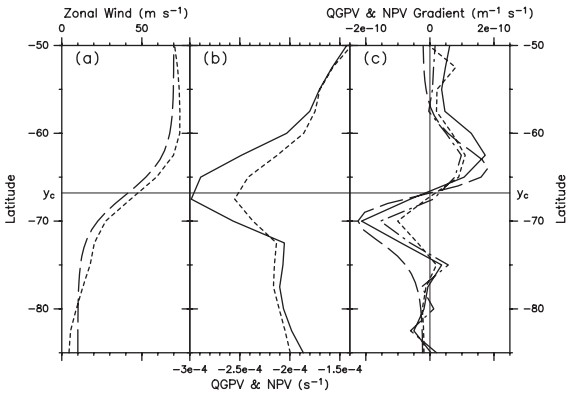

Fig. 11. Latitudinal distributions of (a) zonal wind at 10 hPa (dotted) averaged over the longitude region of 90°W–30°E at 1200 UT on 27 June 2002 and a hyperbolic tangent profile of zonal wind (dashed) given by (6), (b) NPV at 800 K (solid) and QGPV at 10 hPa (dotted) averaged over 90°W–30°E at 1200 UT on 27 June 2002, and (c) NPV gradient at 800 K (solid), QGPV gradient (dotted) and negative zonal wind curvature (dashed-dotted) at 10 hPa averaged over 90°W–30°E at 1200 UT on 27 June 2002, QGPV gradients for $s = 2.2$ (dashed). A thin solid line represents the critical latitude (y_c), where the QGPV gradients in (4) and (7) are zero.

vature. Thus $\beta^* \equiv \beta - \rho_0^{-1}(\rho_0 \varepsilon \bar{u}_z)_z$ is assumed constant in (4).

The QGPV distribution does not exactly accord with the Ertel's potential vorticity distribution when the quasigeostrophic approximation is invalid. In order to directly compare QGPV with potential vorticity, a potential vorticity normalized by $S(\theta) \equiv -g(d\theta_0/dp)_{\theta_0=\theta}$ (where θ_0 is a potential temperature of the reference state) is computed, and referred to as NPV (Juckes 1999). NPV is conserved following the adiabatic and frictionless motion as well as potential vorticity, and has the same unit (s^{-1}) as QGPV. Solid lines in Figs. 11b and 11c represent NPV and NPV gradient at 800 K averaged over the reference longitude region, respectively. The latitudinal variations of NPV and NPV gradient are similar to, but larger than those of QGPV and QGPV gradient in the latitude region of 60°S–70°S. Then a parameter s in (4) is taken to mimic the NPV gradient in the following:

$$\frac{d^2\Psi}{dy^2} + \left(\frac{s(\beta^* - \bar{u}_{yy})}{\bar{u} - c} - k^2\right)\Psi = 0. \tag{7}$$

The QGPV distribution for the case of $s = 2.2$ and $\beta^* = -10^{-11}$ m^{-1} s^{-1} in (7) is shown by a dashed line in Fig. 11c. It accords well with that of NPV gradient at 800 K.

5.2 *Neutral and unstable modes*

The non-singular neutral mode solution in (7) is analytically obtained under the condition that the phase velocity of the neutral mode is equal to the zonal wind velocity at the latitude with zero QGPV gradient (i.e., $\beta^* - \bar{u}_{yy} = 0$ when $\bar{u} - c = 0$). The zonal wind velocity at the latitude with zero QGPV gradient is given by (cf., Dickinson 1973; Kuo 1973)

$$\bar{u} = \frac{U_{max} - U_0}{2}(1 + c^*) + U_0, \tag{8}$$

$$c^* = \frac{2}{\sqrt{3}} \cos\left(\frac{\lambda + 2n\pi}{3}\right), \quad n = 2, 3 \tag{9}$$

$$\lambda = \cos^{-1}\left(\frac{\sqrt{27}}{2}B\right), \quad B \equiv \frac{\beta^* L_y^2}{U_{max} - U_0}.$$

The neutral mode solutions in the cases of $n = 2$ and 3, are associated with the zero QGPV gradients around the latitudes of 66.8°S and 57°S, respectively. Here we focus on the zero QGPV gradient around the latitude of 66.8°S ($n = 2$), which corresponds to the potential vorticity minimum in the observation. This latitude (y_c) is hereafter referred to as the "critical latitude", and shown by a thin solid line in Fig. 11. The latitudinal structure of stream function (Ψ), and a zonal wavenumber of the neutral mode (k_c), are analytically obtained as (cf., Dickinson 1973; Kuo 1973)

$$\Psi(y) = \exp\left(\frac{-c^*(y - y_0)}{L_y}\right) \operatorname{sech}\left(\frac{y - y_0}{L_y}\right), \tag{10}$$

$$k_c L_y = \sqrt{s(1 - c^{*2})}. \tag{11}$$

A zonal wavelength of the neutral mode ($2\pi/k_c$) for the case of $s = 2.2$ is about 2100 km (i.e., 3100 km for the case of $s = 1$). The stream function (Ψ) has a single peak at $y \approx 67.2$°S, which is located slightly poleward of the potential vorticity minimum. These features are in

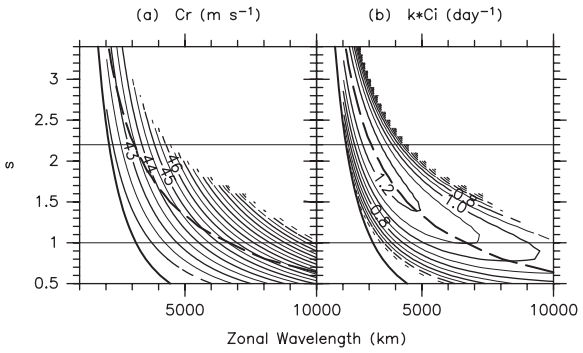

Fig. 12. (a) Ground-based phase velocity and (b) growth rate of unstable modes as a function of zonal wavelength and s. Contour intervals are (a) 0.5 m s^{-1} and (b) 0.1 day^{-1}. Thick dashed and solid lines represent the most unstable mode and the neutral mode at each value of s, respectively. Thin solid lines represent $s = 1$ and 2.2. Regions with growth rates smaller than 0.2 day^{-1} are not drawn.

good agreement with the features of the observed short-period disturbance.

The ground-based phase velocity and growth rate of unstable modes in (7) are numerically computed following Dickinson and Clare (1973). Figures 12a and 12b show the ground-based phase velocity, and growth rate of unstable modes, as a function of zonal wavelength and s. Thick solid and dashed lines in Fig. 12 represent the neutral modes obtained analytically and the most unstable modes, respectively. Unstable modes exist only in the region of zonal wavelength longer than that of the neutral mode. The zonal wavelength and the growth rate of the most unstable mode get shorter and larger, respectively, as s increases. The zonal wavelength of the most unstable mode in the case of $s = 1$ is about 7000 km, and even in the case of $s = 2.2$, it is about 3000 km, which is still longer than the observation. The phase velocity of the most unstable mode relative to the background zonal wind at the critical latitude is 1–3 m s^{-1}.

Figures 13a and 13b show horizontal structures of Ψ of the most unstable and neutral modes, in the case of $s = 2.2$. While Ψ of the most unstable mode has a large phase tilt with latitude against the background horizontal wind shear between $Y = 500$ and -500 km, Ψ of the neutral mode has no phase tilt with latitude. Figure 13c shows latitudinal profiles of $|\Psi|$ of the most unstable and neutral modes in the case of $s = 2.2$. The most unstable mode has two maxima on both sides of the midpoint ($Y = 0$ km in Fig. 13). To the contrary, the neutral mode is maximized slightly poleward of the midpoint ($Y \approx 20$ km) as mentioned earlier, though it is not clear in Fig. 13c. Therefore, the latitudinal structure of the observed short-

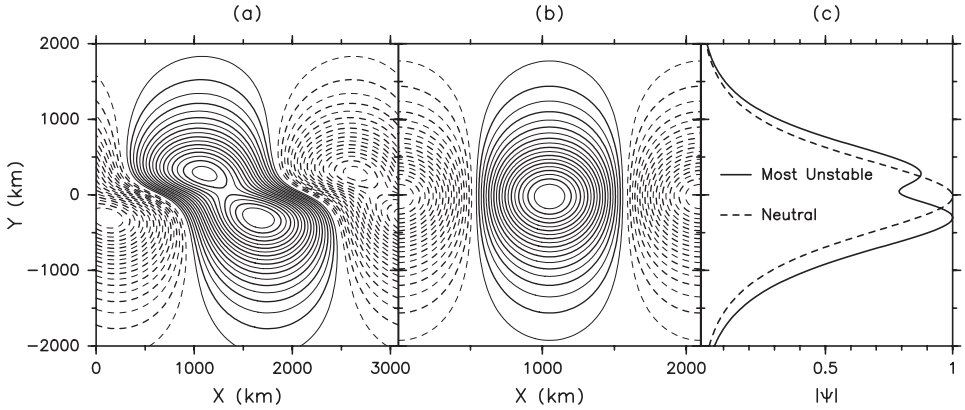

Fig. 13. Horizontal distributions of Ψ of (a) the most unstable and (b) neutral modes, and (c) latitudinal distributions of $|\Psi|$ of (solid) the most unstable and (dotted) neutral modes in the case of $s = 2.2$. Solid and dotted lines in (a) and (b) represent positive and negative values of Ψ, respectively.

period disturbance agrees with those of the neutral mode both in phase and magnitude, much better than those of the most unstable mode.

6. Summary and concluding remarks

An intensive radiosonde observation was performed at Syowa Station (39.6°E, 69°S) in the time period from 20 through 30 June 2002. A disturbance with a period of 12–15 h and a nearly barotropic structure was observed above a height of 22 km on 27 and 28 June 2002. The result of the hodograph analysis indicated that the short-period disturbance was unlikely due to an inertia-gravity wave. Since a similar wavelike structure is seen in the ECMWF operational analysis data, the structure of the short-period disturbance was examined in detail using the ECMWF data. It was shown that the short-period disturbance had a zonal wavelength of about 2000 km, and a horizontal phase velocity of about 40 m s^{-1}. These features are similar to those of the short-period disturbance analyzed in Tomikawa and Sato (2003), which are localized around the polar vortex edge with large potential vorticity gradients. However, the observed short-period disturbance was propagating along the potential vorticity minimum region, where the potential vorticity gradient was zero. A necessary condition for the barotropic instability is satisfied at the potential vorticity minimum region, where the positive and negative potential vorticity gradient regions are lying side-by-side. However, from an analysis using a QGPV equation in a background zonal flow similar to the actual one, it was found that the observed short-period disturbance has characteristics consistent with a neutral mode in the barotropically unstable background flow, rather than an unstable mode, as listed below.

1. A horizontal wavelength of about 2000 km,
2. a horizontal phase velocity equal to the background horizontal wind velocity at the potential vorticity minimum,
3. a latitudinal structure of the meridional wind disturbance, whose amplitude is maximized slightly poleward of the potential vorticity minimum.

This study is one of the few observational reports of a neutral wave existing in such an unstable atmospheric condition. However, it is unlikely that such a neutral wave is a dominant short-period phenomenon in the winter polar stratosphere, because most short-period disturbances are associated with large potential vorticity gradients around the polar vortex edge, as shown in Tomikawa and Sato (2003).

The reason why the neutral wave dominates the unstable wave in the barotropically unstable background flow remains to be answered. First, the effect of zonal asymmetry of the background flow should be taken into consideration. The well-known Rayleigh's criterion for the barotropic instability assumes the zonally-symmetric background flow. The region with the strong contrast of positive and negative potential vorticity gradients was confined to the limited longitude region, in which the short-period disturbance was dominant. The barotropic instability around the zonally-asymmetric polar vortex deformed by the planetary wave activity has been examined in previous studies (Matsuno and Hirota 1966; Hirota 1967; Frederiksen 1982). However, they did not consider the effect of the zonal asymmetry on the instability of small-scale and short-period disturbances. On the other hand, the planetary wave breaking around the winter polar vortex makes a locally unstable region, called "filament". However, the instability associated with such a filament hardly occurs, because a strain field produced by the wave breaking suppresses the instability (Dritschel et al. 1991). As another mechanism suppressing the barotropic instability, Pfister (1979) and Hartmann (1983) suggested the effect of a strong vertical shear of the polar-night jet, which decreases the growth rate of the barotropic instability by rearrangement of the kinetic energy in the vertical. The divergence of horizontal winds, which is neglected in section 5.2, might also contribute to the suppression of barotropic instability. To clarify which is a primary factor for the suppression of the barotropic instability is beyond the scope of this paper and would be a good topic for future work.

A project to construct the first Antarctic MST (Mesosphere-Stratosphere-Troposphere)/IS (Incoherent Scatter) radar at Syowa Station is proceeding (Program of the Antarctic Syowa MST/IS radar; see http://pansy.nipr.ac.jp for details). This radar has an outstanding ability

to capture three-dimensional winds in the troposphere and lower stratosphere, with high accuracy (about 0.1 m s^{-1}) and with high temporal (about 1 minute) and vertical (75 m) resolution. Thus, this project would improve significantly our understanding of dynamics for short-period disturbances in the polar stratosphere as examined in this study.

Acknowledgments

The authors thank Theodore G. Shepherd at the University of Toronto for his helpful comments and suggestions. The data used in this paper were provided by ECMWF, and the GFD-DENNOU Library was used for drawing the figures. This research is supported by Grant-in-Aid for Scientific Research (B)(2) 12440126 of the Ministry of Education, Culture, Sports, Science and Technology, Japan. The first author (YT) is supported by Research Fellowships of the Japan Society for the Promotion of Science for Young Scientists.

References

Andrews, D.G., J.R. Holton, and C.B. Leovy, 1987: *Middle Atmosphere Dynamics*, Academic Press, San Diego, Calif. 489 pp.

Charney, J.G. and P.G. Drazin, 1961: Propagation of planetary-scale disturbances from the lower into the upper atmosphere. *J. Geophys. Res.*, **66**, 83–109.

Dickinson, R.E. and F.J. Clare, 1973: Numerical study of the unstable modes of a hyperbolic-tangent barotropic shear flow. *J. Atmos. Sci.*, **30**, 1035–1049.

———, 1973: Baroclinic instability of an unbounded zonal shear flow in a compressible atmosphere. *J. Atmos. Sci.*, **30**, 1520–1527.

Dritschel, D.G., P.H. Haynes, M.N. Juckes, and T.G. Shepherd, 1991: The stability of a two-dimensional vorticity filament under uniform strain. *J. Fluid Mech.*, **230**, 647–665.

Frederiksen, J.S., 1982: Instability of the three-dimensional distorted polar vortex at the onset of the sudden warming. *J. Atmos. Sci.*, **39**, 2313–2329.

Hartmann, D.L., 1979: Baroclinic instability of realistic zonal-mean states to planetary waves. *J. Atmos. Sci.*, **36**, 2336–2349.

———, 1983: Barotropic instability of the polar night jet stream. *J. Atmos. Sci.*, **40**, 817–835.

Hirota, I., 1967: Dynamic instability of the stratosphere polar vortex. *J. Meteor. Soc. Japan*, **45**, 409–421.

Hoskins, B.J., M.E. McIntyre, and A.W. Robertson, 1985: On the use and significance of isentropic potential vorticity maps. *Quart. J. Roy. Meteor. Soc.*, **111**, 877–946.

Juckes, M., 1999: The structure of idealized upper-tropospheric shear lines. *J. Atmos. Sci.*, **56**, 2830–2845.

Kalnay, E., M. Kanamitsu, R. Kistler, W. Collins, D. Deaven, L. Gandin, M. Iredell, S. Saha, G. White, J. Woollen, Y. Zhu, M. Chelliah, W. Ebisuzaki, W. Higgins, J. Janowiak, K.C. Mo, C. Ropelewski, J. Wang, A. Leetmaa, R. Reynolds, R. Jenne, and D. Joseph, 1996: The NCEP/NCAR 40-year reanalysis project. *Bull. Amer. Meteor. Soc.*, **77**, 437–471.

Kuo, H.L., 1949: Dynamic instability of two-dimensional non-divergent flow in a barotropic atmosphere. *J. Meteor.*, **6**, 105–122.

———, 1973: Dynamics of quasigeostrophic flows and instability theory. *Adv. Appl. Mech.*, **13**, 247–330.

Leovy, C.B. and P.J. Webster, 1976: Stratospheric long waves: Comparison of thermal structures in the northern and southern hemispheres. *J. Atmos. Sci.*, **33**, 1624–1638.

Manney, G.L., T.R. Nathan, and J.L. Stanford, 1988: Barotropic stability of realistic stratospheric jets. *J. Atmos. Sci.*, **45**, 2545–2555.

Matsuno, T. and I. Hirota, 1966: On the dynamical stability of the polar vortex in wintertime. *J. Meteor. Soc. Japan*, **44**, 122–128.

Pfister, L., 1979: A theoretical study of three-dimensional barotropic instability with applications to the upper stratosphere. *J. Atmos. Sci.*, **36**, 908–920.

Rayleigh, Lord, 1880: On the stability or instability of certain fluid motions. *Scientific Papers*, **3**, Cambridge University Press, 594–596.

Sato, K., D.J. O'Sullivan, and T.J. Dunkerton, 1997: Low-frequency inertia-gravity waves in the stratosphere revealed by three-week continuous observation with the MU radar. *Geophys. Res. Lett.*, **24**(14), 1739–1742.

Scinocca, J.F. and P.H. Haynes, 1998: Dynamical forcing of stratospheric planetary waves by tropospheric baroclinic eddies. *J. Atmos. Sci.*, **55**, 2361–2392.

Tomikawa, Y., K. Sato, K. Kita, M. Fujiwara, M. Yamamori, and T. Sano, 2002: Formation of an ozone lamina due to differential advection revealed by intensive observations. *J. Geophys. Res.*, **107**(D10), doi:10.1029/2001JD000386.

——— and ———, 2003: Trapped waves in the edge region of stratospheric polar vortices. *J. Geophys. Res.*, **108**(D2), 4047, doi:10.1029/2002JD002579.

——— and ———, 2005: Design of the NIPR trajec-

tory model. *Polar Meteorol. Glaciol.*, **19**, 120–137.

Yoshiki, M. and K. Sato, 2000: A statistical study of gravity waves in the polar regions based on operational radiosonde data. *J. Geophys. Res.*, **105**(D14), 17995–18011.

———, N. Kizu, and K. Sato, 2005: Seasonal variation in characteristics of gravity waves in the Antarctic lower stratosphere revealed by three-hourly radiosonde observation data at Syowa Station, in preparation.